Atomistic Modeling of entropy-stabilized binary alloys

Preprint · April 2023

DOI: 10.13140/RG.2.2.32606.51526

4 authors, including:

Rafshan Ul Atik
Indian Institute of Technology Madras
1 PUBLICATION **0** CITATIONS
SEE PROFILE

Satyesh Kumar Yadav
Indian Institute of Technology Madras
74 PUBLICATIONS **925** CITATIONS
SEE PROFILE

Atomistic Modeling of entropy-stabilized binary alloys

Rafshan Ul Atik[1], Sufyan M. Shaikh[2], Hitanshu Sachania[3], and Satyesh K. Yadav*[4]

[1,2,3,4]Department of Metallurgical and Materials Engineering, Indian Institute of Technology Madras, Chennai, 600036, Tamil Nadu, India
[4]Center for Atomistic Modeling and Materials Design, Indian Institute of Technology Madras, Chennai, 600036, Tamil Nadu, India

Abstract

The primary factor believed to account for the phase stability of single-phase high entropy alloys is the configurational entropy of mixing. An increase in the number of elements elevates the configurational entropy due to various ways of randomly distributing non-identical constituent species in the lattice. Nevertheless, recent studies have suggested that the dominance of configurational entropy in the phase stability is questionable and it might only constitute a portion of a broader concept. Role of non-configurational entropies with particular emphasis on the dominant vibrational entropy must be investigated when attempting to explicate the stability of high entropy alloys. Present study proposes to find the subtle balance of vibrational and configurational entropy and enthalpy of mixing, and their role in the stability of the simpler binary system of W-Re alloy with first-principle based phonon calculation using density functional theory. Current work focuses on to demonstrate that the stabilizing effect of vibrational entropy on entropy-stabilized binary W-50%Re and W-25%Re alloy, despite having a high enthalpy of mixing, is more significant in the formation of a single-phase solid solution than configurational entropy. In this work, we further calculate the percentage contribution of the vibrational entropy to the total entropy of mixing as a function of temperature for W-50%Re and W-25%Re alloy. We also report the comparison among the vibrational entropy values of pure W, pure Re, W-50%Re and W-25%Re alloy with varying temperature. To facilitate the computational design of single phase high entropy alloys, we suggest to consider vibrational entropy as a means of phase stability besides configurational entropy by demonstrating its significance for the stability of binary alloys.

*corresponding author

1 Introduction

1.1 Ni-Based Superalloys

Nickel-based superalloys are known for their ability to bear loads at extremely high temperatures, up to 85% of their melting point, which makes them particularly well-suited for demanding high temperature structural applications, like manufacturing industrial turbine blades (30 % in weight) and in the hottest sections of gas turbine aero-engines (55 % in weight). [1] The attainment of an increase in matrix strength occurs through addition of different soluble elements, which are likely to include chromium, tungsten, cobalt, molybdenum, rhenium and ruthenium. The distortion of lattice caused by the misfit generated from different atomic radii of constituent elements inhibits dislocation movement. Thus Nickel-based superalloys usually combine high strength, creep strength, fracture toughness, oxidation and corrosion resistance during service at elevated temperatures.
The application of superalloys at elevated temperatures is restricted due to their solvus and melting temperatures. To cope with the extreme working conditions in modern gas turbines, where the turbine entry temperature (1650°C) surpasses the incipient melting temperature (1330°C) of superalloys, [1] clever surface engineered thermal barrier coatings (TBCs) has been implemented. These coatings, which typically have a thickness of $100 - 300$ mm, can reduce the temperature on the superalloy surface by up to 200°C.
The efficiency of an engine is dependent on the highest pressure and temperature attained at the core's center. Though there has been a remarkable improvement in engine efficiency, coupled with a reduction in weight with the aid of improved materials and cooling technologies, the need to boost the efficiency and performance of modern jet engines is still an elusive goal that has been driving most of the global aero-engine development companies to look for alternative materials.

1.2 Refractory High Entropy Alloys (RHEA)

Refractory multi-principal element alloys (RHEA) are a promising material for high-temperature structural applications beyond Ni-based superalloys. Initially introduced in 2010, RHEA quickly caught attention due to their ability to maintain high strength even at extreme temperatures of up to 1600°C. The first two RHEAs, MoNbTaW and MoNbTaVW, [2] consisted of five refractory elements, including molybdenum, niobium, tantalum, vanadium, and tungsten. However, subsequent alloys have been developed from a wider range of nine elements, including Group IV (titanium, zirconium, and hafnium), Group V (vanadium, niobium, and tantalum), and Group VI (chromium, molybdenum, and tungsten). According to the original definition, RHEA are alloys composed of five or more principal elements with each element's concentration ranging between 5 and 35 atomic percent. Some refractory multi-component alloys comprise of four main components, while some contain an element with a concentration exceeding 35%. Such alloys, which encompass HEA, are recognized as refractory complex concentrated alloys (RCCA) or refractory multiprincipal element alloys.[3]
However, none of the currently reported Transition Metal (TM) High-Entropy Alloys (HEA) have demonstrated elevated temperature properties that surpass advanced Ni-based superalloys. Many of the reported RHEA and RCCA are of BCC structure and the most common phase found among the reported RHEA and RCCA is disordered BCC. [3] Similar to any BCC materials, RHEA also faces the problem of insufficient compressive ductility at temperatures

lower than or equal to 600°C, except for the equimolar HfNbTaTiZr alloy and some of its related composition. Due to the varying sizes of all solute atoms, the lattice structure becomes highly distorted in a multi-element lattice. This local lattice distortions in BCC RHEA make it harder for dislocations to move through the lattice. [4] Poor room temperature compressive ductility, inadequate oxidation resistance, and high density have limited the use of various BCC RHEA. Consequently, there is a significant aim to develop strategies to ductilize RHEA that possess both high temperature strength and ductility at room temperature.

1.3 Ductilizing RHEA

Several methodologies have been documented in the literature that discuss enhancing the intrinsic pliability of RHEA. Intrinsic ductility is defined by the intrinsic ductility parameter (D) [5] as follows:

$$D = \frac{\gamma_s}{\gamma_{usfe}} \tag{1}$$

$$D > 1 \implies \text{Intrinsically ductile}$$

$$D < 1 \implies \text{Intrinsically brittle}$$

where γ_{usfe} is the unstable stacking fault energy and γ_s is the surface energy needed to create new crack surface. Unstable stacking fault energy can be calculated using density functional theory (DFT) using the following relation,

$$\gamma_{usfe} = \frac{\mathrm{E_{faulted}} - \mathrm{E_{pristine}}}{\text{Area of Plane}}$$

where the $\mathrm{E_{faulted}}$ is the energy of supercell having a stacking fault and the $\mathrm{E_{pristine}}$ is the energy of pristine supercell [6].

The alteration of the balance between strength and ductility in RHEA can be achieved by adding or substituting different elements. According to [7], the concept of valence electron concentration (VEC) suggests that BCC RHEAs composed of subgroup IV, V, and VI metals are intrinsically ductile if their VEC < 4.5 and intrinsically brittle if VEC $>= 4.5$. Addition of subgroup IV elements (Hf, Ti,Zr) reduces VEC and enhances the alloy's deformability, while the addition of subgroups V and VI elements, along with Al, often increases the alloy's strength but reduces its ductility [3]. However, VEC approach does not consider the thermodynamic stability of the alloys.

Enhancing the production of RHEA at a reduced temperature is feasible through the addition of elements that decrease γ_{usfe} of the alloys from their composition averaged value ($\Delta\gamma_{usfe}$) and thereby increasing the deformability of the alloy. This can be achieved by incorporating HCP metals of subgroup IV (Ti, Zr, Hf) which have low γ_{usfe}. [6] found strong inverse correlation between $\Delta\gamma_{usfe}$ and enthalpy of mixing ($\Delta_{\mathrm{mix}}\mathrm{H}$), which states that positive $\Delta_{\mathrm{mix}}\mathrm{H}$ decreases unstable stacking fault energy from their composition averaged values, which in turn improves the intrinsic ductility of the alloy. Alloys having positive enthalpy of mixing experiences repulsion among its constituent species, which makes the alloys more deformable by facilitating dislocation glide.

Traditionally, ductilization of W has been done by addition of HCP element Re [8], [9], even though it increases VEC of the alloy. Considering thermodynamic stability of WRe refractory alloys, 35% reduction in unstable stacking fault energy from their composition averaged value,

$\Delta\gamma_{usfe}$, has been reported for equiatomic BCC WRe [6]. Strong inverse correlation between $\Delta\gamma_{usfe}$ and enthalpy of formation (Δ_fE) suggests that equiatomic BCC WRe alloy should have very large positive Δ_{mix}H. In fact, equiatomic WRe shows an extreme case of having the most positive enthalpy of formation Δ_fE of 0.0994 eV/atom [6]. Such high values of Δ_fE suggests that entropic contribution must be sufficient for the equiatomic BCC WRe alloy to be stable as a single phase solid solution.

1.4 Entropic contribution

For any random substitutional solid solution, the stability of a phase under constant pressure is determined by Gibbs energy of mixing Δ_{mix}G, which is expressed as,

$$\Delta_{\text{mix}}\text{G} = \Delta_{\text{mix}}\text{H} - \text{T}\Delta_{\text{mix}}\text{S} \tag{2}$$

where Δ_{mix}H is the enthalpy of mixing and Δ_{mix}S is the entropy of mixing of the alloy. Phase stability under constant volume is dictated by Helmholtz energy of mixing Δ_{mix}A, which is given as,

$$\Delta_{\text{mix}}\text{A} = \Delta_{\text{mix}}\text{E} - \text{T}\Delta_{\text{mix}}\text{S} \tag{3}$$

Here Δ_{mix}E denotes the internal energy of mixing. Alloys having large positive Δ_{mix}H are prone to phase separation and can even show the occurrence of miscibility gap at low temperature. On the contrary, large negative Δ_{mix}H can result into ordered alloys or intermetallics. Selective preference for the formation of like bonds and phase separation tendency of the alloys having large enthalpy of mixing can be prevented if the alloys possess large entropy of mixing. Contributions to the total entropy of mixing of for an alloy come from configurational ($\Delta_{\text{mix}}\text{S}^{\text{conf}}$), vibrational (($\Delta_{\text{mix}}\text{S}^{\text{vib}}$))and electronic entropy of mixing (($\Delta_{\text{mix}}\text{S}^{\text{elec}}$)). Combining all the mentioned contributions to the total entropy of mixing, the equation for Gibbs energy of mixing can rewritten as,

$$\Delta_{\text{mix}}\text{G} = \Delta_{\text{mix}}\text{H} - \text{T}(\Delta_{\text{mix}}\text{S}^{\text{conf}} + \Delta_{\text{mix}}\text{S}^{\text{vib}} + \Delta_{\text{mix}}\text{S}^{\text{elec}}) \tag{4}$$

.

The primary factor believed to account for the phase stability of single-phase RHEA is the configurational entropy of mixing. An increase in the number of elements elevates the configurational entropy due to various ways of randomly distributing non-identical constituent species in the lattice. Nevertheless, recent studies have suggested that the role of configurational entropy might only constitute a portion of a broader concept [10]. Role of non-configurational entropies with particular emphasis on the dominant vibrational entropy must be investigated when attempting to explicate the stabilty of WRe binary alloys. Present study hopes to find the subtle balance of vibrational and configurational entropy and enthalpy of mixing, and their role in the stability of the simpler refractory binary system of W-Re alloy with first-principle based phonon calculation using density functional theory (DFT). Current work focuses on demonstrate that the stabilizing effect of vibrational entropy on entropy-stabilized refractory W-Re alloy, despite having a high enthalpy of mixing, is more significant in the formation of a single-phase solid solution than configurational entropy.

2 Methodology

2.1 Special quasirandom structures

Special quasirandom structures (SQS) provide the most accurate representation of the chemical disorder of a true disordered state for a given number of atoms. SQS are considered optimal since they are designed to match a specified set of correlations between neighboring site occupations with the corresponding correlation of the fully disordered state. A 64 atom BCC primitive SQS with equiatomic composition of W and Re and $W_{0.75}Re_{0.25}$ have been generated using MCSQS (Monte Carlo Special Quasirandom Structure) code as implemented by Alloy Theoretic Automated Toolkit (ATAT) [11, 12]. Perfect match of the correlation functions of pairs, triplets and quadruplets, where no pair of atoms are separated longer than the lattice parameter of BCC WRe unit cell (which is the second nearest neighbour distance of any atom in a BCC unit cell), has been obtained between the generated structure with the infinite substitutional random alloys. Generated SQS have been visualized using VESTA [13] software.

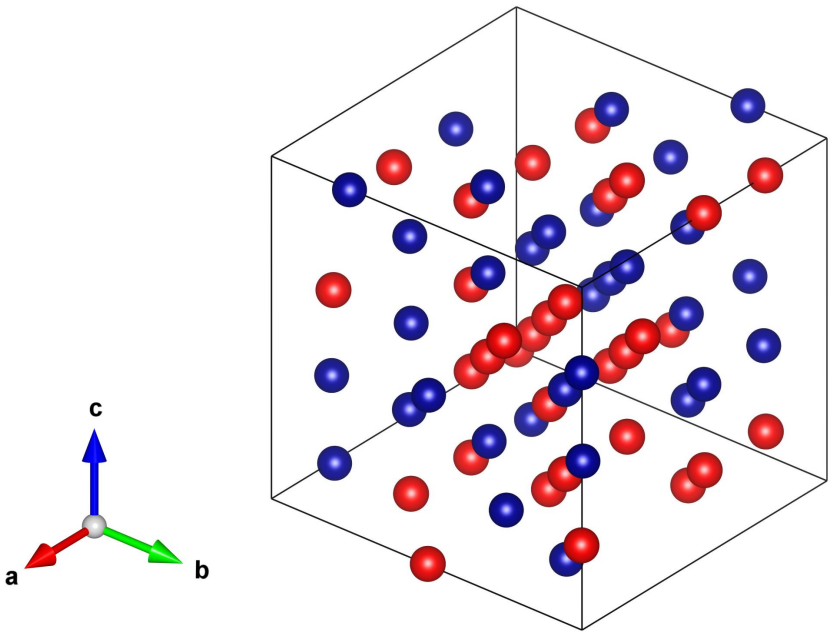

Figure 1: A 64 atom relaxed $W_{0.5}Re_{0.5}$ BCC primitive SQS. Red atoms represent W, blue atoms represent Re.

2.2 Lattice dynamics

Harmonic phonon energy of the crystal [14] at constant volume is obtained from from the canonical distribution in statistical mechanics for phonon and is given as:

$$U_{\text{phonon}} = \sum_{\mathbf{q},\nu} \hbar\omega(\mathbf{q},\nu) \left[\frac{1}{2} + \left(\exp\left(\hbar\omega(\mathbf{q},\nu)/k_{\text{B}}T\right) - 1\right)^{-1}\right] \tag{5}$$

where the summation runs over all wave vectors, $\mathbf{q}$, and over all branches in the dispersion diagram, ν. $\omega(\mathbf{q},\nu)$ is the angular frequency at $\mathbf{q}$ and ν, T is the absolute temperature, k_B

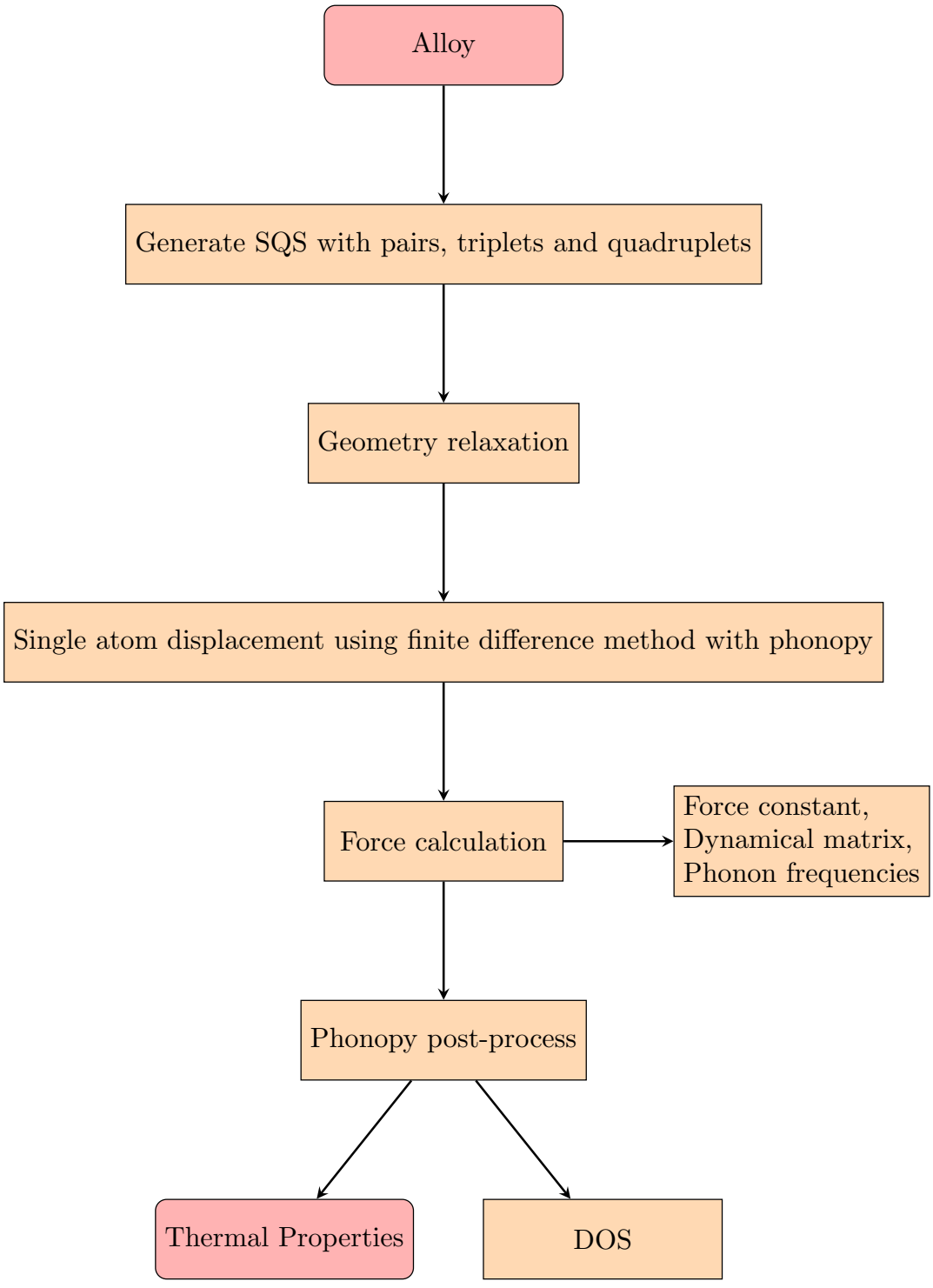

Figure 2: Workflow

is the Boltzmann constant and $\hbar$ is the reduced Planck constant. Temperature-independent term in the total energy expression is called the zero-point energy (ZPE) of the phonon modes. Total energy at constant volume can also be calculated by directly evaluating phonon density of states as a function of angular frequency and subsequently multiplying it by the average energy of a single mode at a given frequency and then integrating over all frequencies obtained from the dispersion curves calculated over a fine grid of wave vectors within the first Brillouin zone.
The heat capacity at constant volume, C_V, is then equal to:

$$\begin{aligned} C_V &= \left(\frac{\partial E}{\partial T}\right)_V \\ &= \sum_{\mathbf{q},\nu} k_{\mathrm{B}} \left(\frac{\hbar\omega(\mathbf{q},\nu)}{k_{\mathrm{B}}T}\right)^2 \frac{\exp\left(\hbar\omega(\mathbf{q},\nu)/k_{\mathrm{B}}T\right)}{\left[\exp\left(\hbar\omega(\mathbf{q},\nu)/k_{\mathrm{B}}T\right)-1\right]^2} \end{aligned} \tag{6}$$

Vibrational entropy, S^{vib} at constant volume is given as:

$$S^{vib} = -k_{\mathrm{B}} \sum_{\mathbf{q},\nu} \ln\left[1-\exp\left(-\hbar\omega(\mathbf{q},\nu)/k_{\mathrm{B}}T\right)\right] - \frac{1}{T}\sum_{\mathbf{q},\nu} \frac{\hbar\omega(\mathbf{q},\nu)}{\exp\left(\hbar\omega(\mathbf{q},\nu)/k_{\mathrm{B}}T\right)-1} \tag{7}$$

Phonon contribution to the free energy at constant volume or Helmholtz energy for a unary system can then be evaluated using the above expressions as:

$$\begin{aligned} A_{\text{phonon}} &= U_{\text{phonon}} - TS^{vib} \\ &= \frac{1}{2}\sum_{\mathbf{k},v} \hbar\omega(\mathbf{k},v) + k_{\mathrm{B}}T \sum_{\mathbf{k},v} \ln\left[1-\exp\left(-\hbar\omega(\mathbf{k},v)/k_{\mathrm{B}}T\right)\right] \end{aligned} \tag{8}$$

It is important to note that the above expressions are applicable only under the assumption that the crystal follows a harmonic model for constant volume, which does not account for anharmonic effects such as thermal expansion. Nonetheless, experiments are typically conducted under constant pressure conditions as it is challenging to design an experiment that precludes thermal expansion.
The volume-dependence of phonon properties can be introduced by using quasi-harmonic approximation of phonons [15], where the harmonic approximation is applied at each volume independently. It is observed that the frequencies of a system tend to decrease as the volume of the system increases. This trend can be explained by the fact that interatomic forces generally decrease as bond lengths increase, which in turn leads to a decrease in frequency. As the angular frequency decreases, vibrational entropy at that particular volume is going to increase, which further stabilises the system leading to a net thermal expansion. The structure of a crystal at any temperature will be in a state of equilibrium with the lowest free energy. Therefore, it is possible to simulate the temperature dependence of a crystal structure by finding the minimum of its free energy with respect to volume of the supercell. Thus Gibbs free energy G may be written as:

$$G(T,p) = \min_V \left[U(V) + A_{\text{phonon}}(T;V) + pV\right] \tag{9}$$

where V and p are the volume and pressure, respectively, and $U(V)$ is the total energy of electronic structure at constant volume, the value of which can be obtained after geometric

relaxation using DFT. Heat capacity at constant pressure is derived from $G(T,p)$ by:

$$C_P(T,p) = -T\frac{\partial^2 G(T,p)}{\partial T^2} = T\frac{\partial V(T,p)}{\partial T}\frac{\partial S(T;V)}{\partial V}\bigg|_{V=V(T,p)} + C_V[T,V(T,p)] \tag{10}$$

where $V(T,p)$ is the equilibrium volume at T and p.

2.3 First-principles calculations

W-50%Re and W-25%Re SQS structures containing 64 atom have been prepared as an input file for geometric relaxation in the framework of DFT using Vienna Ab-initio Simulation Package (VASP) with plane-wave basis cut-off of 520 eV and projector augmented wave (PAW) pseudopotentials [16–18]. 5d and 6s electrons for W and 5p, 5d and 6s electrons for Re are treated as valence electrons; rest all are kept frozen. Exchange correlation functional used for calculation is Perdew-Burke-Erzernhoff generalized gradient approximation (PBE-GGA) [19, 20]. Sampling of the Brillouin zone is achieved through the Monkhorst-Pack scheme [21] using an automatically generated mesh with k-point spacing of less than $2\pi \times 0.03$ Å^{-1} for all the calculations. To perform the relaxation process, Methfessel-Paxton of first order with a smearing width of 0.2 eV is utilized [22], and relaxation continues until the forces on the atoms fall below 0.5 meV/Å. The resultant relaxed structure is utilized as an input supercell for phonon calculation through the implementation of the finite difference method as carried out in phonopy [15, 23]. For each 64 atom WRe alloys, 384 displaced structures have been generated with the displacement for each atom being 0.01Å in x-, y- and z-direction. Strict energy convergence criteria (10^{-7} eV) is used for electronic relaxation of each displaced supercell. The computation of force constants, dynamical matrix, phonon frequencies, and eigenvectors with q-point grid of $64 \times 64 \times 64$ is performed after the calculation of Hellmann-Feynman forces on the atoms for each random alloy via the utilization of phonopy. Helmholtz energy as a function of temperature is then calculated on a $1\times1\times1$ supercell using the Parlinski-Li-Kawazoe method [24].

To get thermal properties at constant pressure, QHA is utilized by calculating $U(V)$ and $A_{\text{phonon}}(T;V)$ at 7 different volumes. Thermodynamic functions for the all the volume points are then fitted to a third order Birch-Murnaghan equation of state (EOS) to get the equilibrium volume and isothermal bulk modulus for each random alloy and pure elements at $p = 0$. Gibbs free energies at finite temperatures is evaluated from the minimum values of the fitted thermodynamic functions. Augmentation of equilibrium volume indicates thermal expansion. $\frac{\partial V(T,p)}{\partial T}$ is calculated by numerical differentiation. C_V and and S are fitted with respect to volume with a polynomial function [25] to get C_P values at different temperatures using 10.

3 Results & discussion

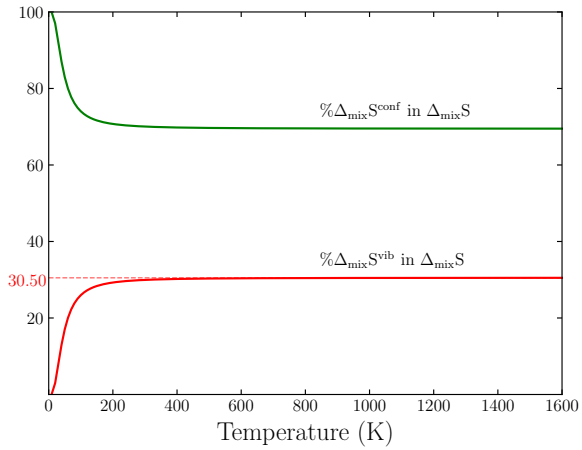

(a) $W_{0.5}Re_{0.5}$

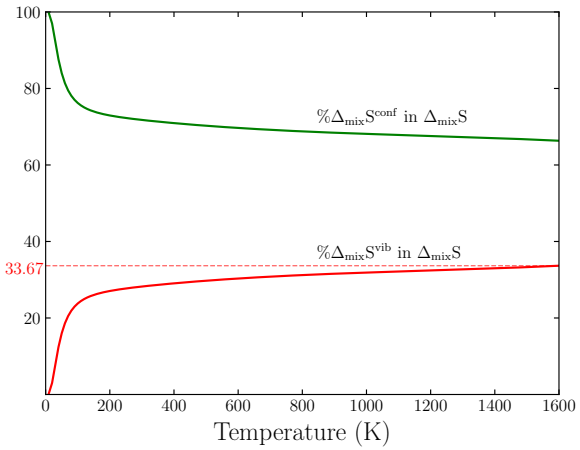

(b) $W_{0.5}Re_{0.5}$

Figure 3: Percentages of configurational entropy of mixing ($\Delta_{mix}S^{conf}$) and vibrational entropy of mixing ($\Delta_{mix}S^{vib}$) in the total entropy of mixing ($\Delta_{mix}S$) of $W_{0.5}Re_{0.5}$ alloy under (a) harmonic and (b) quasi-harmonic approximation.

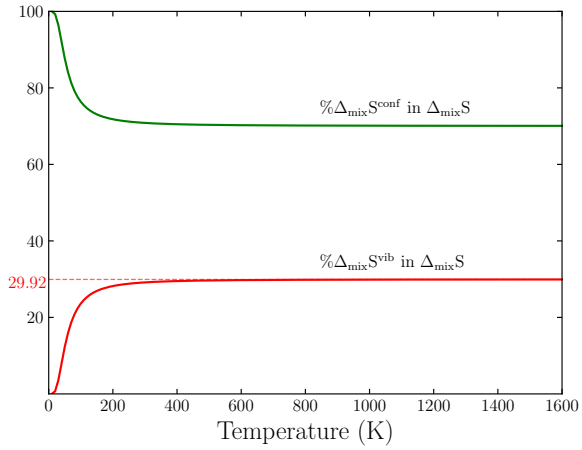

(a) $W_{0.75}Re_{0.75}$

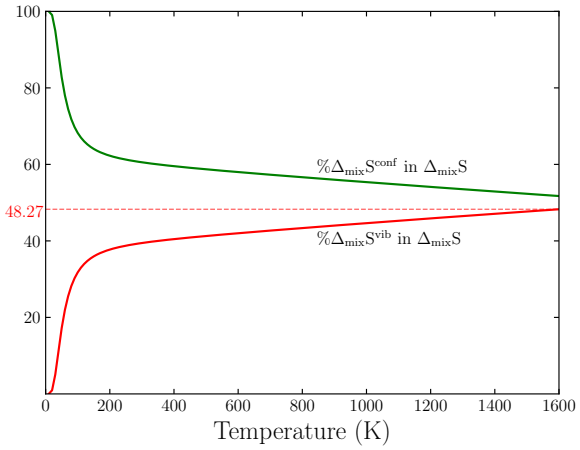

(b) $W_{0.75}Re_{0.75}$

Figure 4: Percentages of configurational entropy of mixing ($\Delta_{mix}S^{conf}$) and vibrational entropy of mixing ($\Delta_{mix}S^{vib}$) in the total entropy of mixing ($\Delta_{mix}S$) of $W_{0.75}Re_{0.25}$ alloy under (a) harmonic and (b) quasi-harmonic approximation.

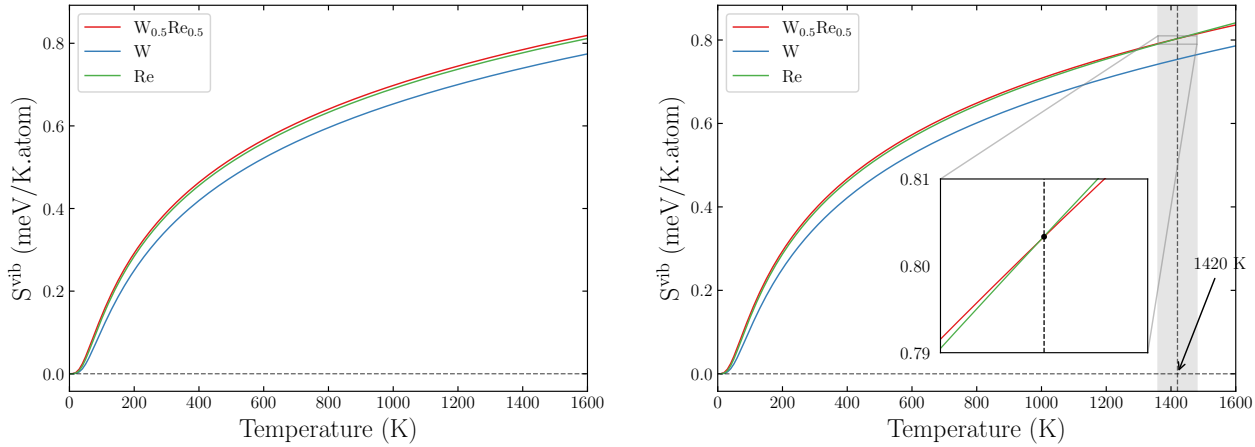

(a) **(b)**

Figure 5: Temperature dependence of vibrational entropy (S^{vib}) for pure W, pure Re and $W_{0.5}Re_{0.5}$ alloy under (a) harmonic and (b) quasi-harmonic approximation.

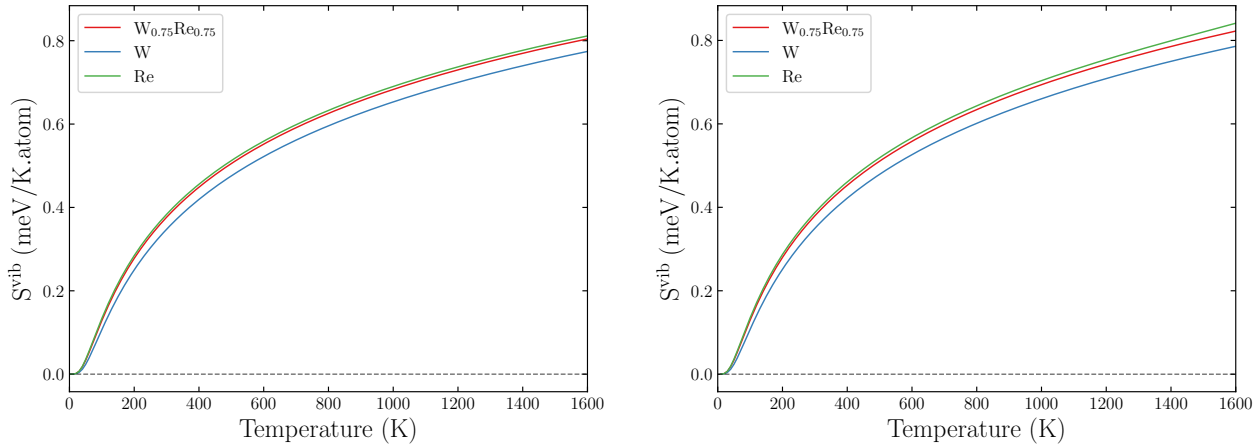

(a) **(b)**

Figure 6: Temperature dependence of vibrational entropy (S^{vib}) for pure W, pure Re and $W_{0.75}Re_{0.25}$ alloy under (a) harmonic and (b) quasi-harmonic approximation.

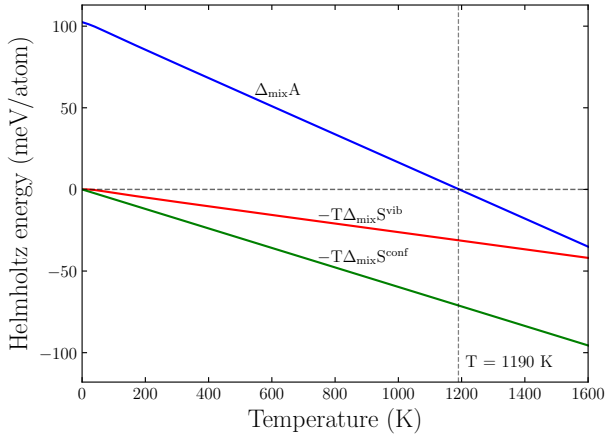

(a) $W_{0.5}Re_{0.5}$

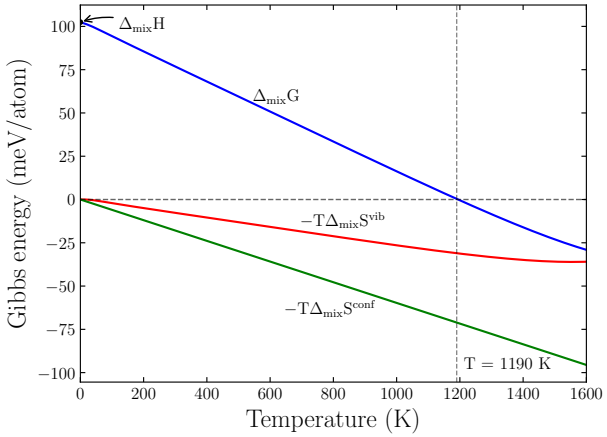

(b) $W_{0.5}Re_{0.5}$

Figure 7: (a) Temperature dependence of Helmholtz energy of mixing ($\Delta_{mix}A$) for $W_{0.5}Re_{0.5}$ alloy showing vibrational ($-T\Delta_{mix}S^{vib}$) and configurational ($-T\Delta_{mix}S^{conf}$) entropic contributions under harmonic approximation, (b) Temperature dependence of Gibbs energy of mixing ($\Delta_{mix}G$) for $W_{0.5}Re_{0.5}$ alloy showing vibrational ($-T\Delta_{mix}S^{vib}$) and configurational ($-T\Delta_{mix}S^{conf}$) entropic contributions under quasi-harmonic approximation.

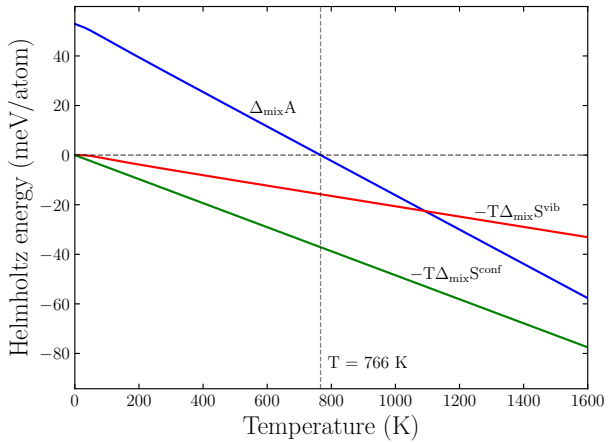

(a) $W_{0.75}Re_{0.75}$

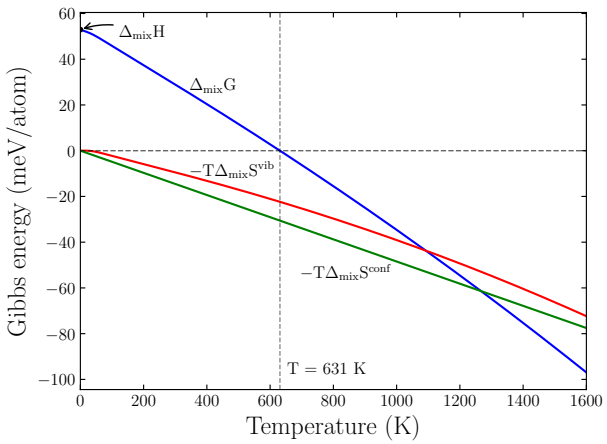

(b) $W_{0.75}Re_{0.25}$

Figure 8: (a) Temperature dependence of Helmholtz energy of mixing ($\Delta_{mix}A$) for $W_{0.75}Re_{0.25}$ alloy showing vibrational ($-T\Delta_{mix}S^{vib}$) and configurational ($-T\Delta_{mix}S^{conf}$) entropic contributions under harmonic approximation, (b) Temperature dependence of Gibbs energy of mixing ($\Delta_{mix}G$) for $W_{0.75}Re_{0.25}$ alloy showing vibrational ($-T\Delta_{mix}S^{vib}$) and configurational ($-T\Delta_{mix}S^{conf}$) entropic contributions under quasi-harmonic approximation.

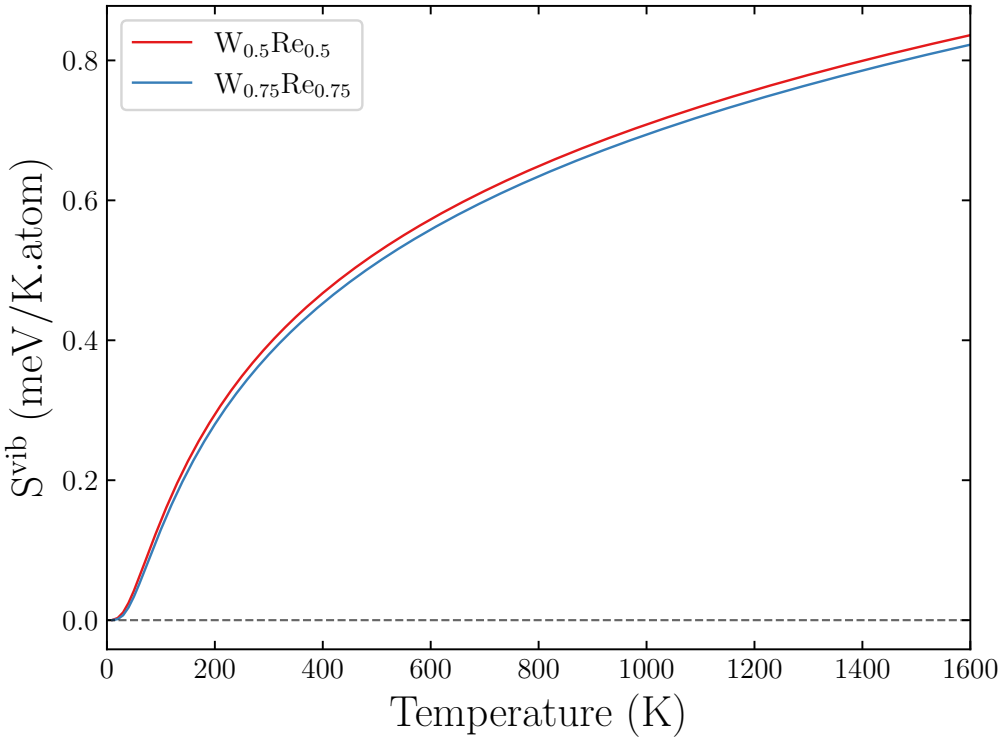

Figure 9: Comparison between the vibrational entropy (S^{vib}) for $W_{0.5}Re_{0.5}$ and $W_{0.75}Re_{0.25}$ alloy under quasi-harmonic approximation.

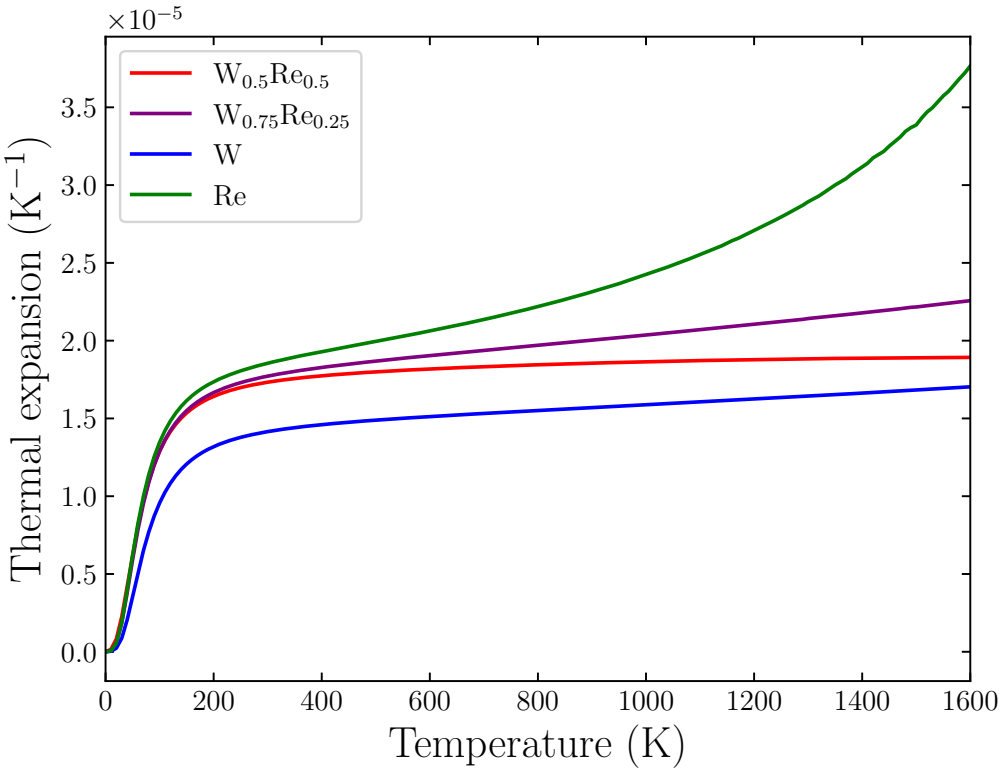

Figure 10: Temperature dependence of coefficient of thermal expansion for pure W, pure Re and $W_{0.5}Re_{0.5}$ alloy.

Bulk modulus values are in agreement with previous experimental and computational results.

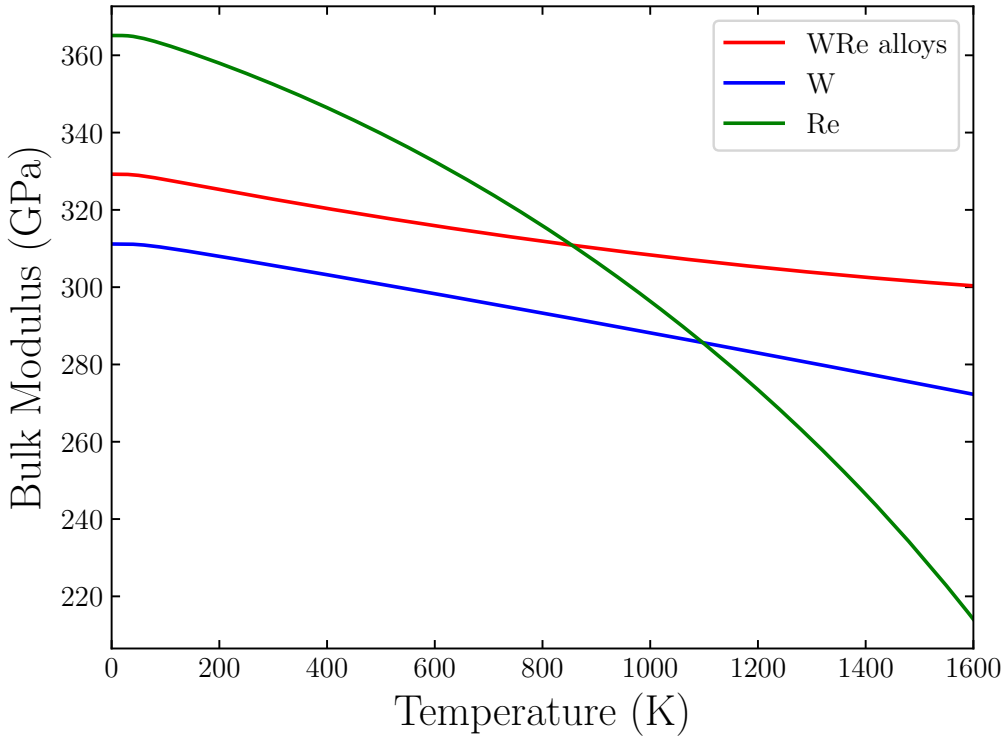

Figure 11: Temperature dependence of bulk modulus for pure W, pure Re and WRe alloys.

Table 1: Comparison of bulk modulus values of Re at room temperature

B (GPa)	**Methods**
336	X-ray diffraction [26]
363.3	Ultrasonic [27]
352.6	X-ray diffraction [28]
383	X-ray diffraction, MD [29]
447	LDA [30]
382	LDA [31]
344	GGA [31]
389	LDA [32]
376	GGA [32]
352.5	GGA (present study)

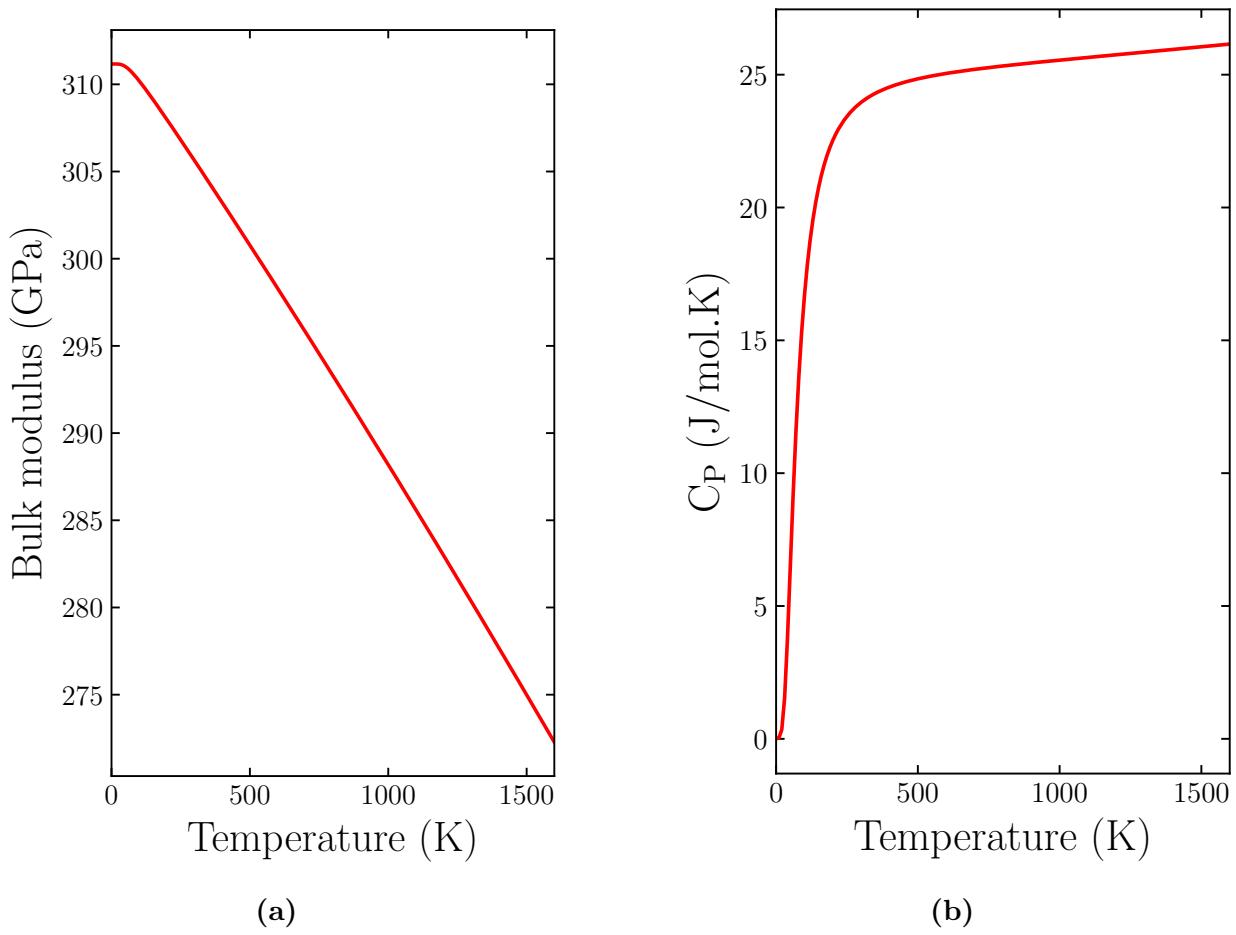

Figure 12: Temperature dependence of (a) bulk modulus and (b) molar heat capacity at constant pressure (C_P) of pure W.

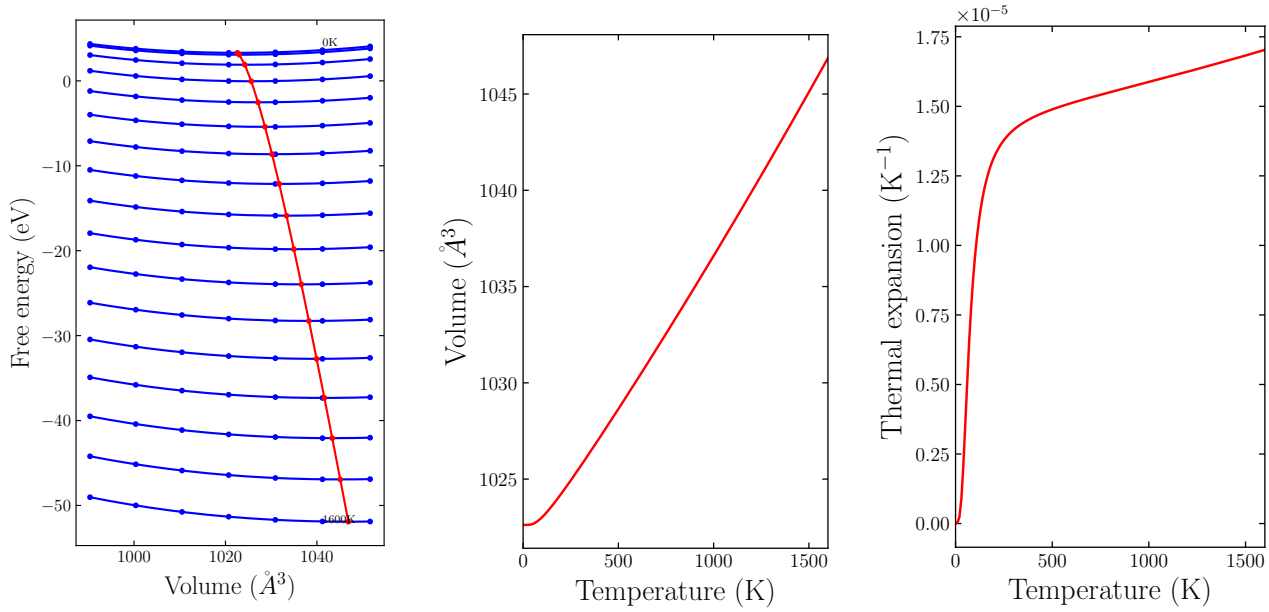

(a) **(b)** **(c)**

Figure 13: (a) Helmholtz energy vs volume plot (b) Volume vs temperature plot (c) Thermal expansion vs temperature plot for pure W

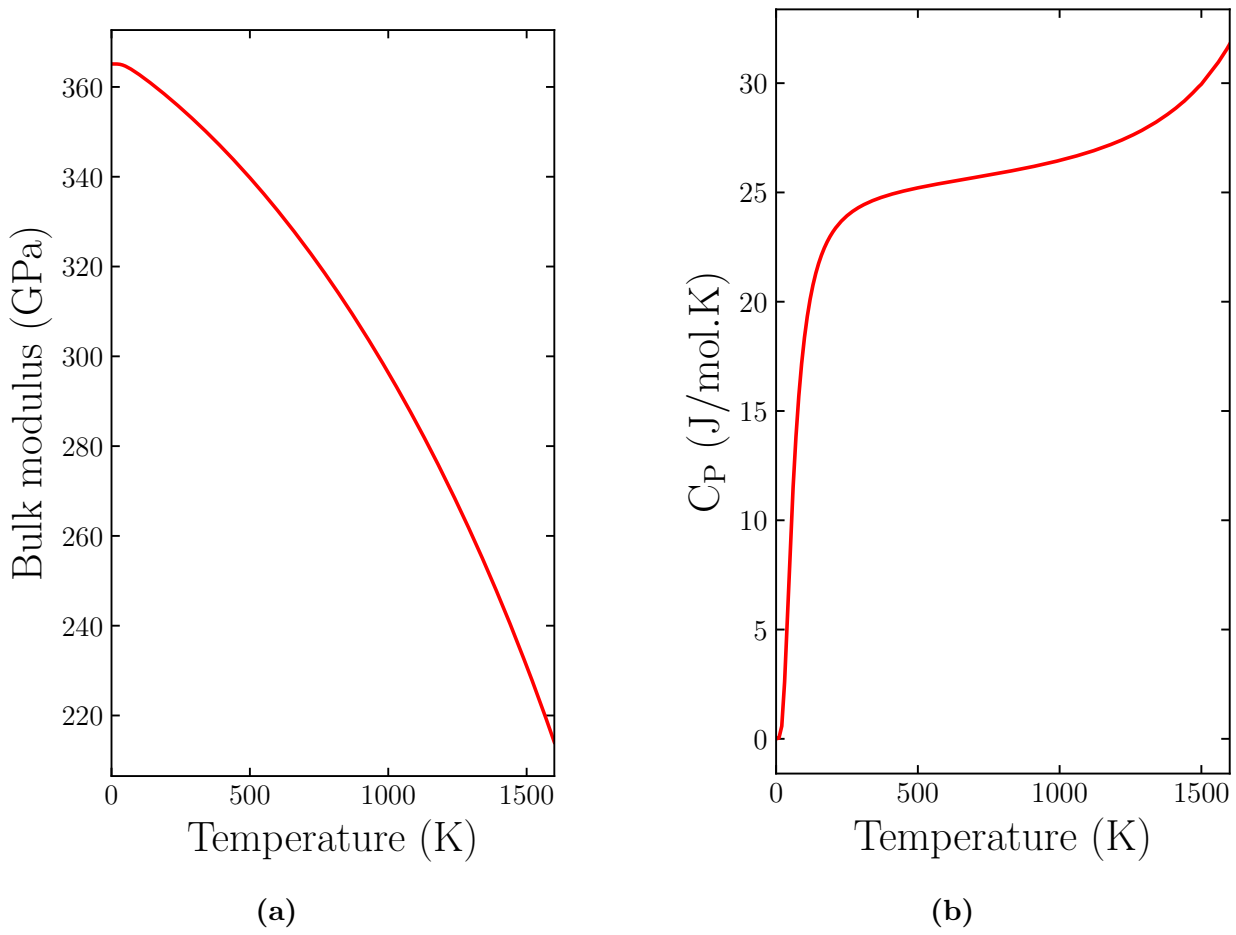

Figure 14: Temperature dependence of (a) bulk modulus and (b) molar heat capacity at constant pressure (C_P) of pure Re.

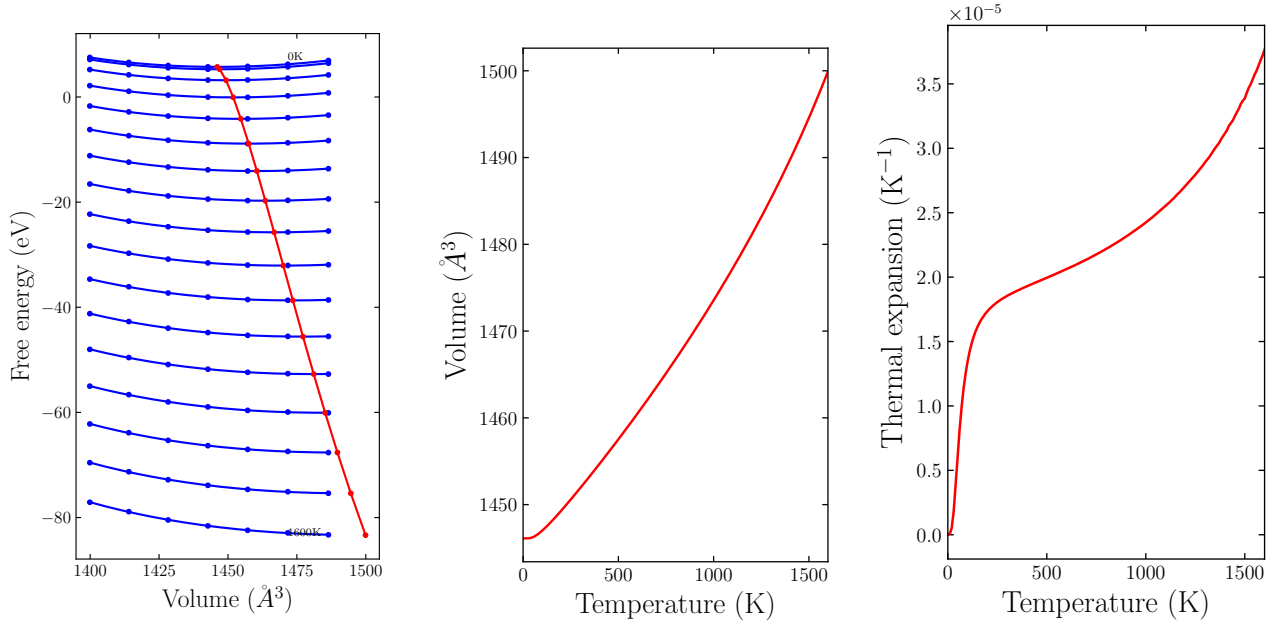

Figure 15: (a) Helmholtz energy vs volume plot (b) Volume vs temperature plot (c) Thermal expansion vs temperature plot for pure Re

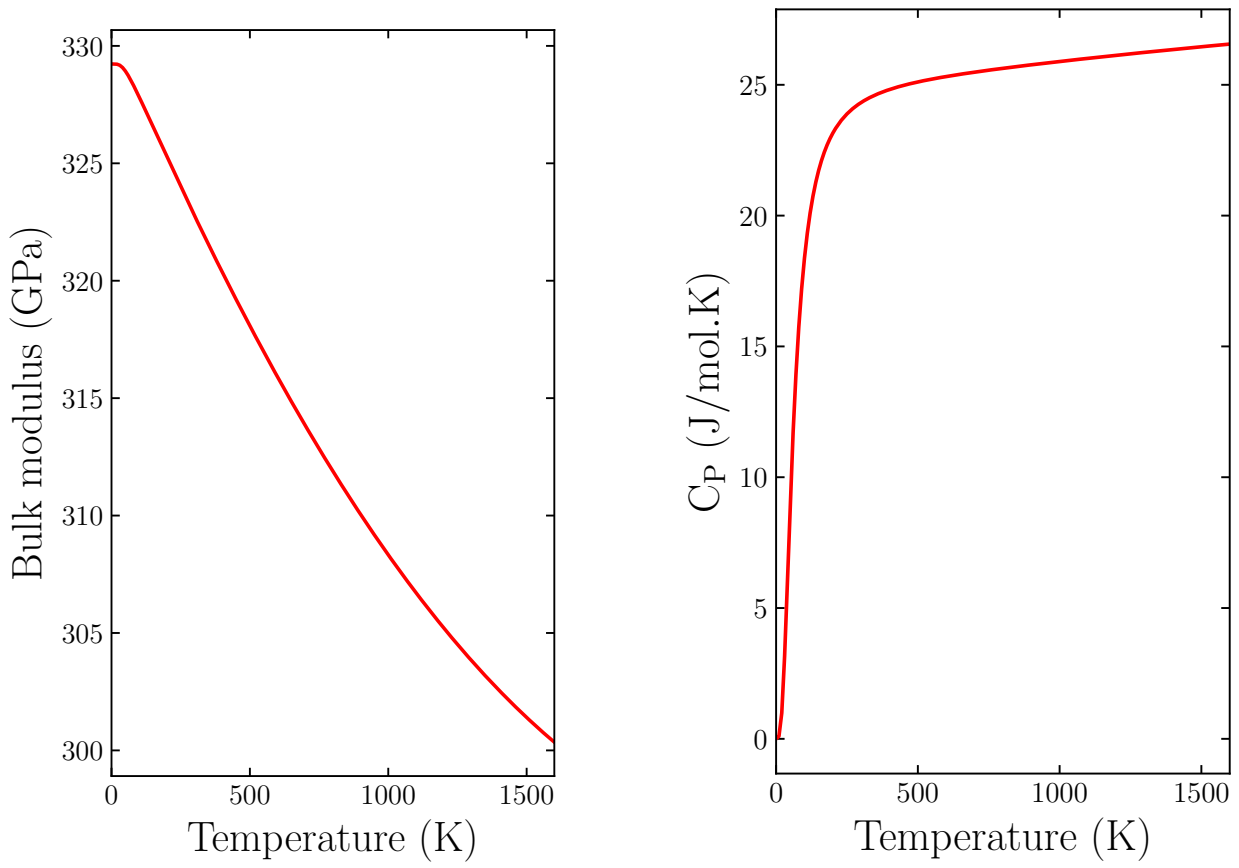

Figure 16: Temperature dependence of (a) bulk modulus and (b) molar heat capacity at constant pressure (C_P) of $W_{0.5}Re_{0.5}$ alloy.

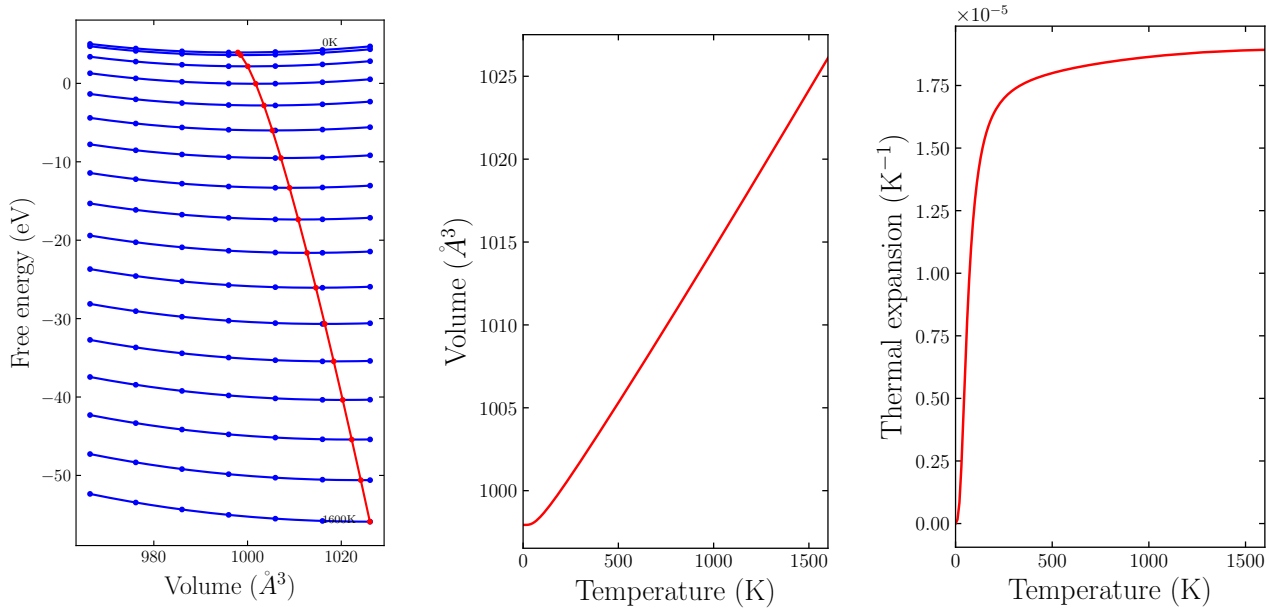

(a) **(b)** **(c)**

Figure 17: (a) Helmholtz energy vs volume plot (b) Volume vs temperature plot (c) Thermal expansion vs temperature plot for $W_{0.5}Re_{0.5}$ alloy

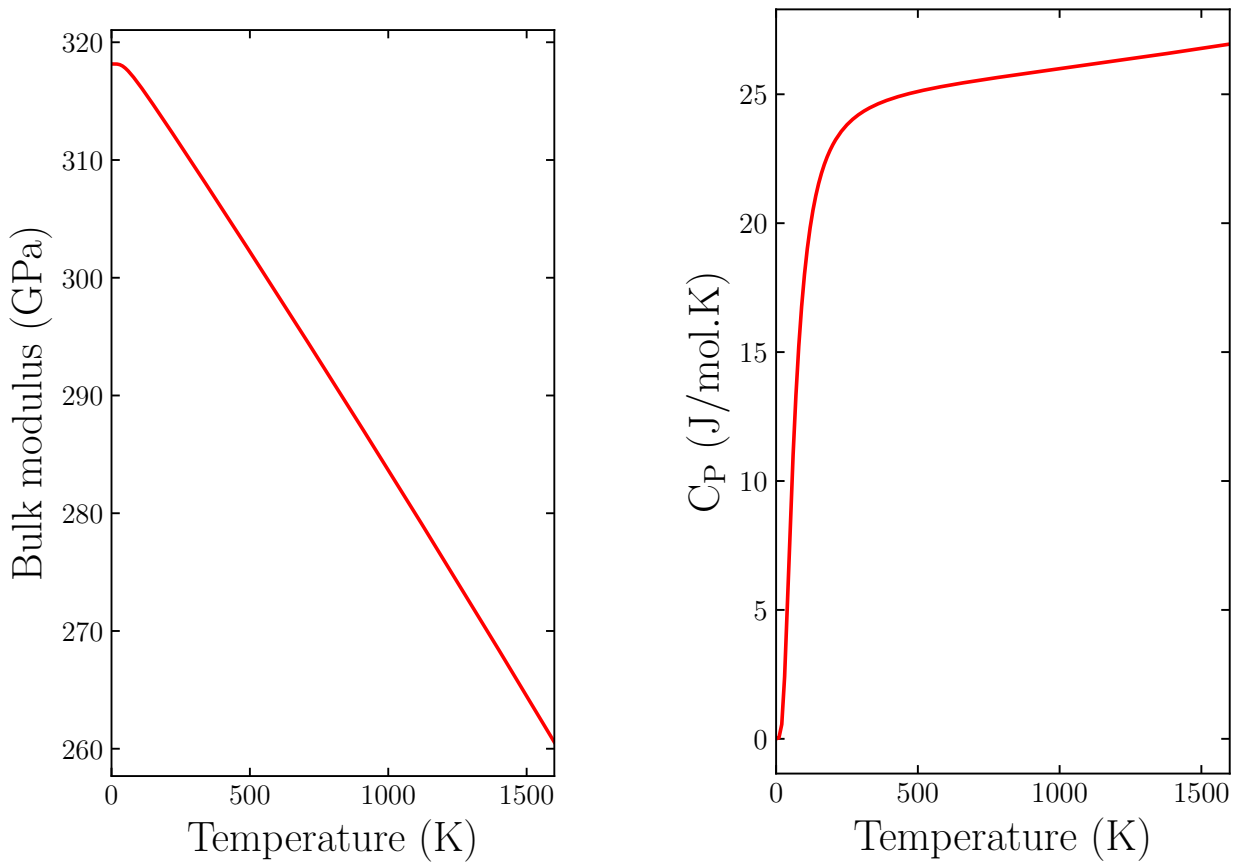

Figure 18: Temperature dependence of (a) bulk modulus and (b) molar heat capacity at constant pressure (C_P) of $W_{0.75}Re_{0.25}$ alloy.

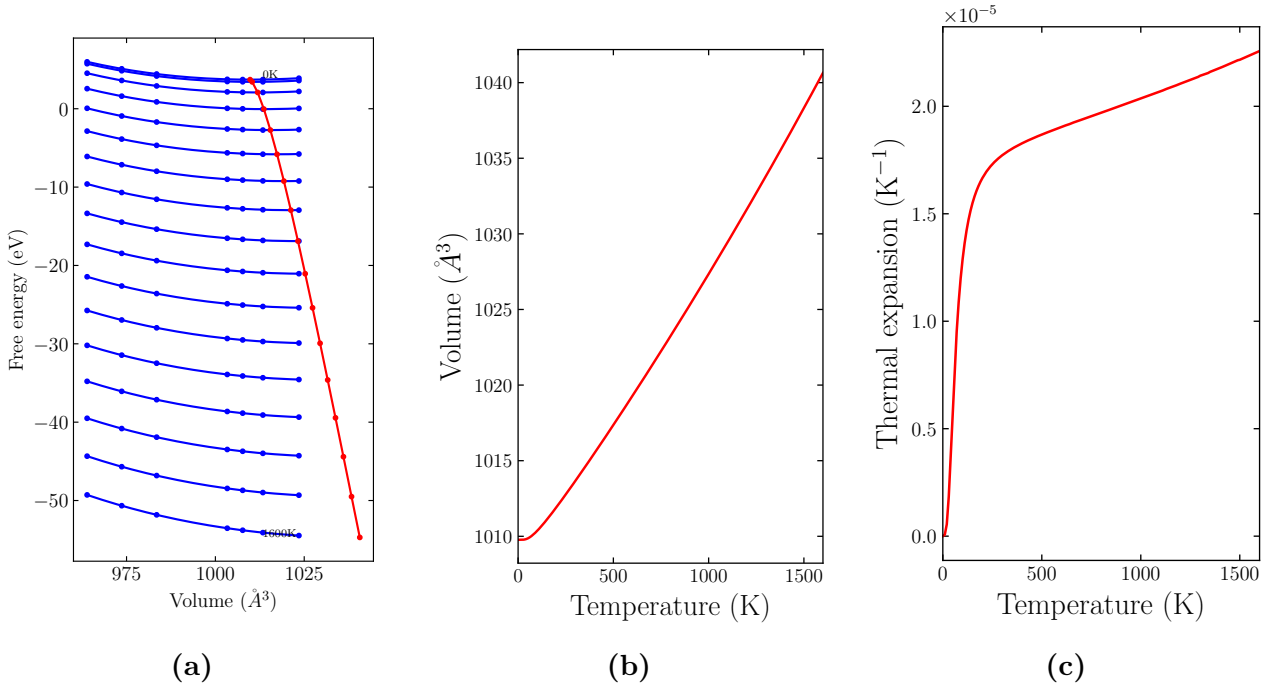

Figure 19: (a) Helmholtz energy vs volume plot (b) Volume vs temperature plot (c) Thermal expansion vs temperature plot for $W_{0.75}Re_{0.25}$ alloy

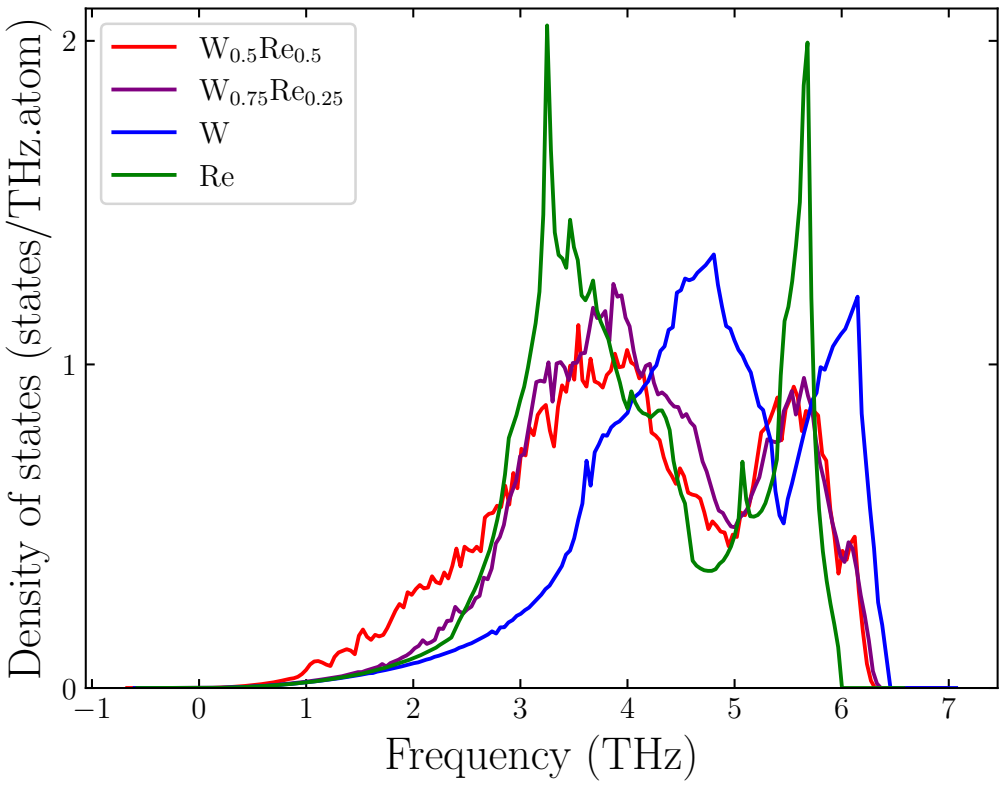

Figure 20: Density of states plot for pure W, pure Re, $W_{0.5}Re_{0.5}$ and $W_{0.75}Re_{0.25}$ alloy.

4 Conclusion

In this work, we have showed using first principle phonon calculations using DFT that vibrational entropy plays major role in stabilization of W-50%Re and W-75%Re. We have reported contribution from vibrational entropy to the total entropy of the mixing, $\sim 34\%$ for W-50%Re and $\sim 48\%$ for W-75%Re at 1600K, which is highest reported so far in the literature. Although data of absolute values of vibrational entropy have been available, entropy of mixing data which truly captures phase stability of any random alloy are sparse. This work attempts to capture quantitative information for the role of vibrational entropy of mixing in the phase stability of binary alloy, which will help to further explicate the single phase of stability in case of high entropy alloys.

References

[1] L. Liu, J. Zhang, C. Ai, Nickel-Based Superalloys, Elsevier, 2021. doi:10.1016/B978-0-12-803581-8.12093-4.

[2] O. Senkov, G. Wilks, D. Miracle, C. Chuang, P. Liaw, Refractory high-entropy alloys, Intermetallics 18 (9) (2010) 1758–1765. doi:https://doi.org/10.1016/j.intermet.2010.05.014.
URL https://www.sciencedirect.com/science/article/pii/S0966979510002475

[3] O. N. Senkov, D. B. Miracle, K. J. Chaput, J. P. Couzinie, Development and exploration of refractory high entropy alloys - a review, Journal of Materials Research 33 (2018) 3092–3128. doi:10.1557/jmr.2018.153.

[4] J. W. Yeh, Recent progress in high-entropy alloys, Annales de Chimie: Science des Materiaux 31 (2006) 633–648. doi:10.3166/acsm.31.633-648.

[5] Y.-J. Hu, A. Sundar, S. Ogata, L. Qi, Screening of generalized stacking fault energies, surface energies and intrinsic ductile potency of refractory multicomponent alloys, Acta Materialia 210 (2021) 116800.

[6] S. M. Shaikh, B. S. Murty, S. K. Yadav, Designing a thermodynamically stable and intrinsically ductile refractory alloy, Journal of Alloys and Compounds 939 (2023) 168597. doi:10.1016/j.jallcom.2022.168597.

[7] S. Sheikh, S. Shafeie, Q. Hu, J. Ahlström, C. Persson, J. Veselỳ, J. Zỳka, U. Klement, S. Guo, Alloy design for intrinsically ductile refractory high-entropy alloys, Journal of applied physics 120 (16) (2016) 164902.

[8] G. Geach, J. Hughes, The alloys of rhenium with molybdenum or with tungsten and having good high temperature properties, in: Plansee Proceedings, Pergamon Press London, 1955, pp. 245–253.

[9] C. Ren, Z. Z. Fang, M. Koopman, B. Butler, J. Paramore, S. Middlemas, Methods for improving ductility of tungsten - a review, International Journal of Refractory Metals and Hard Materials 75 (2018) 170–183. doi:10.1016/j.ijrmhm.2018.04.012.

[10] A. Manzoor, S. Pandey, D. Chakraborty, S. R. Phillpot, D. S. Aidhy, Entropy contributions to phase stability in binary random solid solutions, npj Computational Materials 4 (1) (2018) 47.

[11] A. Van De Walle, M. Asta, G. Ceder, The alloy theoretic automated toolkit: A user guide, Calphad 26 (4) (2002) 539–553.

[12] A. Van de Walle, P. Tiwary, M. De Jong, D. Olmsted, M. Asta, A. Dick, D. Shin, Y. Wang, L.-Q. Chen, Z.-K. Liu, Efficient stochastic generation of special quasirandom structures, Calphad 42 (2013) 13–18.

[13] K. Momma, F. Izumi, Vesta 3 for three-dimensional visualization of crystal, volumetric and morphology data, Journal of applied crystallography 44 (6) (2011) 1272–1276.

[14] M. T. Dove, Introduction to Lattice Dynamics, Cambridge Topics in Mineral Physics and Chemistry, Cambridge University Press, 1993. doi:10.1017/CBO9780511619885.

[15] A. Togo, I. Tanaka, First principles phonon calculations in materials science, Scripta Materialia 108 (2015) 1–5.

[16] G. Kresse, J. Hafner, Ab initio molecular dynamics for liquid metals, Physical review B 47 (1) (1993) 558.

[17] P. E. Blöchl, Projector augmented-wave method, Physical review B 50 (24) (1994) 17953.

[18] G. Kresse, J. Furthmüller, Efficient iterative schemes for ab initio total-energy calculations using a plane-wave basis set, Physical review B 54 (16) (1996) 11169.

[19] J. P. Perdew, K. Burke, M. Ernzerhof, Generalized gradient approximation made simple, Physical review letters 77 (18) (1996) 3865.

[20] G. Kresse, D. Joubert, From ultrasoft pseudopotentials to the projector augmented-wave method, Physical review b 59 (3) (1999) 1758.

[21] H. J. Monkhorst, J. D. Pack, Special points for brillouin-zone integrations, Physical review B 13 (12) (1976) 5188.

[22] M. Methfessel, A. Paxton, High-precision sampling for brillouin-zone integration in metals, Physical Review B 40 (6) (1989) 3616.

[23] A. Togo, First-principles phonon calculations with phonopy and phono3py, Journal of the Physical Society of Japan 92 (1) (2023) 012001.

[24] K. Parlinski, Z. Li, Y. Kawazoe, First-principles determination of the soft mode in cubic zro 2, Physical Review Letters 78 (21) (1997) 4063.

[25] A. Togo, L. Chaput, I. Tanaka, G. Hug, First-principles phonon calculations of thermal expansion in ti 3 sic 2, ti 3 alc 2, and ti 3 gec 2, Physical Review B 81 (17) (2010) 174301.

[26] L.-G. Liu, T. Takahashi, W. A. Bassett, Effect of pressure and temperature on the lattice parameters of rhenium, Journal of Physics and Chemistry of Solids 31 (6) (1970) 1345–1351.

[27] M. H. Manghnani, K. Katahara, E. S. Fisher, Ultrasonic equation of state of rhenium, Physical Review B 9 (4) (1974) 1421.

[28] L. Dubrovinsky, N. Dubrovinskaia, V. B. Prakapenka, A. M. Abakumov, Implementation of micro-ball nanodiamond anvils for high-pressure studies above 6 mbar, Nature communications 3 (1) (2012) 1163.

[29] S. Ono, Equation of state determination for rhenium using first-principles molecular dynamics calculations and high-pressure experiments, Advances in Condensed Matter Physics 2022 (2022).

[30] L. Fast, J. M. Wills, B. Johansson, O. Eriksson, Elastic constants of hexagonal transition metals: Theory, Phys. Rev. B 51 (1995) 17431–17438. doi:10.1103/PhysRevB.51.17431. URL https://link.aps.org/doi/10.1103/PhysRevB.51.17431

[31] G. Steinle-Neumann, L. Stixrude, R. E. Cohen, First-principles elastic constants for the hcp transition metals fe, co, and re at high pressure, Physical Review B 60 (2) (1999) 791.

[32] M.-B. Lv, Y. Cheng, Y.-Y. Qi, G.-F. Ji, C.-G. Piao, Elastic properties and phonon dispersions of rhenium in hexagonal-close-packed structure under pressure from first principles, Physica B: Condensed Matter 407 (4) (2012) 778–783.